IMPACT OF HEAT AND MOISTURE TRANSFER THROUGH A MULTILAYER WALL ON THE COMFORT CONDITIONS OF AN OCCUPIED ROOM

Rudy Bui, Matthieu Labat, Sylvie Lorente

ABSTRACT

Controlling indoor air quality is today a major concern for three main reasons: occupants' comfort, durability and energy performance. Nowadays, most of the technical solutions rely on active methods for air conditioning. However, materials can moderate the indoor relative humidity (RH) variations thanks to their buffering capacity and therefore they may regulate the RH in a passive way. It could be interesting to exploit this property as it is estimated that approximately one third of the moisture generated in a room can be absorbed by the wall surfaces. The factors influencing moisture balance in buildings are: the moisture interactions between indoor air and materials, the HVAC systems, and the indoor moisture sources. The objective of this work is to account for these factors to propose a realistic estimation of the moisture buffering of materials and its impact on the energy consumption and the occupants' comfort.

The first step in achieving this objective is to study the moisture interactions between the environment and the wall materials. Hence, a one-dimensional heat and moisture model at the wall scale is developed in PYTHON by using the capillary pressure as moisture driving potential. Conservation equations for the indoor air will take into account the indoor heat and moisture sources from the occupants' presence which are generated by a multi-agent stochastic simulation tool. Finally, a first estimation of the moisture buffering of materials is proposed. The results highlighted that the use of a hygroscopic material in a wall leads to an important increase in the prediction of the comfort conditions in terms of relative humidity. However, no significant impact on the energy savings was noticed. As hygroscopic materials have an influence on the indoor relative humidity, it could lead to better energy savings if a humidification/dehumidification system is simulated.

INTRODUCTION

Nowadays, the topic of energy savings has become a major concern. New techniques were developed to address it, but they led to new challenges. In building physics, issues related to humidity are drawing attention as it concerns the energy consumption, the durability of materials and the occupants' comfort. Most techniques used to regulate indoor humidity relies on mechanical systems like air-conditioning which are part of Heat, Ventilation and Air-Conditioning systems (HVAC). However, HVAC are the most energy-consuming systems as they represent approximately 50% of the global energy consumption of buildings (Perez-Lombard et al., 2011). On the other hand, hygroscopic materials can absorb or release humidity in a passive way when they are subjected to relative humidity variations in a room (Hameury, 2005): this is

called the moisture buffering. According to Diasty and Fazio (1992), this phenomenon can contribute to as much as one third of the global humidity regulation of the indoor air. Yet, it depends on many parameters like the materials, the indoor air regulation systems and the presence and activities of occupants. Numerical studies conducted to realistically estimate the moisture buffering of materials and evaluate its impact on the energy consumption and the comfort conditions do not usually address all the above parameters with the same level of detail. This may be exemplified in (Barbosa and Mendes, 2008): each of the HVAC system components were modelled in detail, but the simulation did not take into account the presence of occupants in the building. Additionally, (Qin et al., 2011) simulated a whole house in different climate conditions but an ideal heating system was modelled and the occupants' presence was simplified.

Hence, studying heat and moisture transfer through building materials and accounting for detailed indoor boundary conditions (HVAC system and occupants' presence and activities) are of capital importance to propose a realistic estimation of the moisture buffering of materials.

Heat and Moisture Transfer in Building Physics

Heat and moisture transfer have already been studied extensively, starting with Philip and De Vries (1957) and Luikov (1975) work in soil science. The first numerical models, named HAM (Heat, Air and Moisture) were developed in the beginning of the 1990s with the models MATCH (Pedersen, 1990) and WUFI (Künzel, 1995). An exhaustive state of the art can be found in Delgado et al. (2010) who identifies 14 open access models among more than 50 existing models. A more precise description of some of these models is available in Woloszyn and Rode (2008). It accounts for the numerical method, the driving potential for the conservation equations, the modeled physical phenomena and the simulation of a ventilation system. At the building scale, some examples can also be found such as in Tariku et al. (2010) or in Qin et al. (2011). In the latter, the energy and mass balance on the indoor air were included based on the AIRNET model (Walton, 1989).

Indoor Heat and Moisture Sources

Although most heat and moisture transfer models at the wall and the room scale rely on the same physical phenomena, the description of indoor conditions varies from one model to the other. For room scale models, HVAC equipment and indoor heat and moisture sources have to be modelled. In fact, these sources are strictly depending on the use of the building, which also be depicted by occupants' presence and activities. A wide range of approaches can be found in the literature and could be classified in three main groups:

- Constant indoor sources (exemplified in TenWolde and Walker (2001) for moisture production);
- Deterministic representation of the occupants' presence;
- Stochastic approaches.

The use of deterministic scenario is the most common approach. In Qin et al. (2011), an occupant was simulated at night in a residential test house from 8:00 pm to 8:00 am with a metabolic heat gain equal to 500 W and a moisture production equal to 0.5 $g.m^{-3}.h^{-1}$. Similarly, Künzel et al. (2005a) used a moisture production rate of 0.5 $g.m^{-3}.h^{-1}$ with peaks in the morning and evening, i.e 8 $g.m^{-3}.h^{-1}$ from 6:00 to 8:00 am and 4 $g.m^{-3}.h^{-1}$ from 4:00 to 10:00 pm every day.

Though convenient, results from deterministic scenarios differ widely from observed measures. Stochastic models are a viable alternative. In the field of energy performance, Page et al. (2008) proposed a stochastic model of presence relying on Markov chains. His model was then calibrated and validated with on-site measurements. For the activities of occupants, Jaboob (2015) modelled a wide range of activities (use of appliances, cooking, showering, etc.) based on time use surveys data. Haldi and Robinson (2009) developed the occupants' interactions with windows based on 7 years of data provided by sensors installed in a real office building. More recently Labat and Woloszyn (2015) investigated the impact of a stochastic moisture production scheme with an average production rate equal to 87 g/h. They highlighted that the average vapor flux exchanged between the indoor air and the walls was underestimated by 50-80% when a constant moisture production rate was selected. Additionally, using a constant moisture production schedule led to an increase of 10-20% in the prediction of the comfort range.

Objectives

In order to realistically estimate the moisture buffering of materials and its impact on the energy consumption of building and the comfort conditions of occupants, the following methodology was proposed:

1) Solving numerically a coupled heat and moisture transfer problem through a multilayer wall;
2) Modelling the occupants' presence and activities in a stochastic way;
3) Modelling a HVAC system based on the study of a real HVAC system.

To this end, this paper focused on the first two objectives. Firstly, a one-dimensional heat and moisture transfer model is presented. This model is then coupled with a stochastic model of occupants' presence via an interface. Finally, two different walls were simulated and compared: a conventional wall and one made of a hygroscopic material, selected in order to emphasize the moisture buffering effect.

MODELS DESCRIPTION

This section aims to present the different modelling elements (Figure 1):

1) A heat and moisture transfer model (HM model) through a multilayer wall;
2) The exterior boundary conditions;
3) The interior boundary conditions accounting for the impact of occupants' presence in offices.

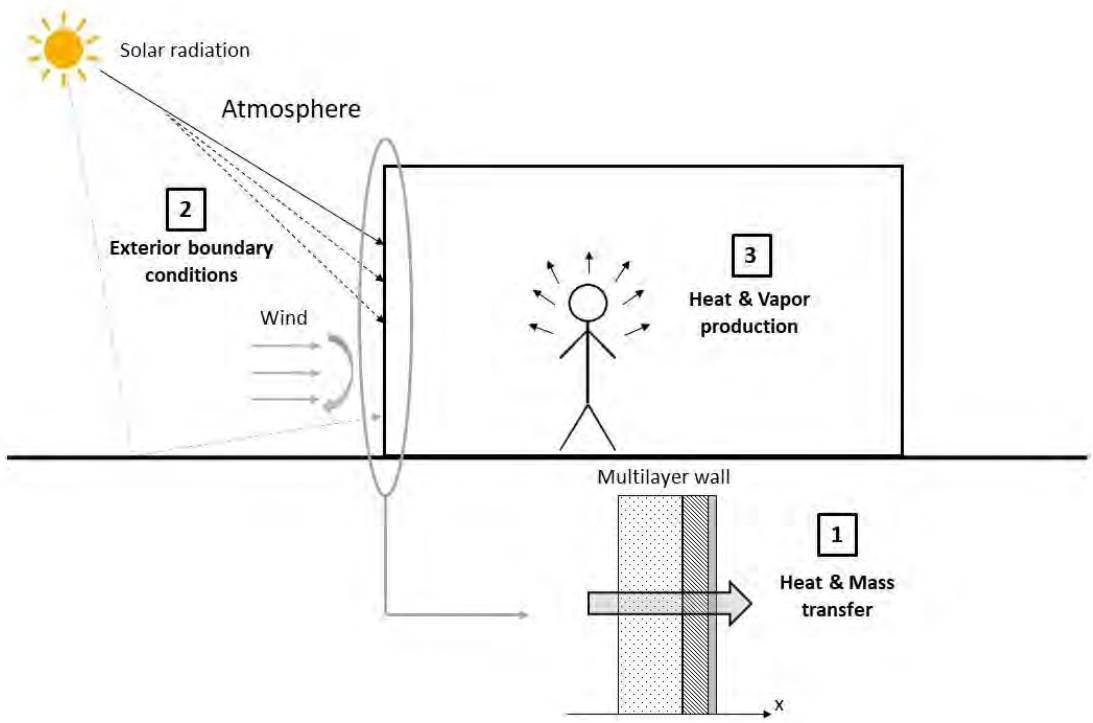

Figure 1: Schematic representation of the different part of the problem

Coupled Heat and Moisture Transfer through a Multilayer Wall

The coupled heat and moisture transfer model presented in this section is governed by one-dimensional set of equations for a porous multi-layer wall (Lorente, 2017). According to the IEA Annex 41 (Woloszyn and Rode, 2007) this model falls under the category "intermediate-grained models". For heat transfer, the temperature is the only driving potential. However, for mass transfer, many potentials can be used: the capillary pressure (Janssen et al., 2007; Li et al., 2009), the logarithm of the capillary pressure (Schellen et al., 2008), the water content (Künzel and Kiesel, 1994), the water vapor pressure (Janssens, 2001), the relative humidity (Tariku et al., 2010), the mass ratio (H.-J. Steeman et al., 2009) can be quoted among others. A comparative study of the driving potentials based on a literature review - not presented here - led to choose the capillary pressure. Firstly it can be qualified as a true potential since it comes directly from Darcy's law. According to Janssen (2014) it also performs better than the other potentials near saturation, making it the most performant potential on the whole range of relative humidity. Finally, it is the dominant choice for simulation of moisture transfer in soil science.

The mass conservation equation account for the water vapor transfer (Fick's diffusion) and the liquid water vapor transfer (Darcy's law):

$$\frac{\partial w}{\partial p_c}\frac{\partial p_c}{\partial t} = -\frac{\partial}{\partial x}\left(\delta_l \frac{\partial p_c}{\partial x} - \delta_v \frac{\partial p_v}{\partial x}\right) \quad \textbf{(1)}$$

where w is the water content of the material (kg/m^3), t is the time (s), δ_l is the liquid water permeability (s), p_c is the capillary pressure (Pa), δ_v is the water vapor permeability (s) and p_v is the water vapor pressure

(Pa). In this case, the air transfer is neglected under the assumption that there is not variation of the total pressure. As the chosen driving potential is the capillary pressure, equation (1) becomes after some mathematics:

$$\frac{\partial w}{\partial p_c}\frac{\partial p_c}{\partial t} = -\frac{\partial}{\partial x}\left[\left(\delta_l + \delta_v \frac{\rho_v}{\rho_l}\right)\frac{\partial p_c}{\partial x} - \delta_v\left(\psi \frac{\partial p_{vsat}}{\partial T} - p_v \frac{\ln\psi}{T}\right)\frac{\partial T}{\partial x}\right] \quad (2)$$

where ρ_l is the liquid water density (kg/m^3), Ψ is the relative humidity (-) and T the temperature (K). The energy conservation equation is governed by the first law of thermodynamics stating that the rate of energy accumulated within the control volume is equal to the net heat transfer of energy by conduction plus the net transfer of energy by fluid flow (Bejan, 2004). Consequently, the energy conservation equation is described by:

$$\left(\rho_s c_s + \sum_i w_i c_{p,i}\right)\frac{\partial T}{\partial t} = k_{mat}\frac{\partial^2 T}{\partial x^2} - \sum_i w_i V_i c_{p,i}\frac{\partial T}{\partial x} - \left[(c_{p,l} - c_{p,v})T - L_v\right]S_l \quad (3)$$

where c is the heat capacity (J/(kg.K)) the subscript s stands for the solid, $i=v$ for vapor or $i=l$ for liquid, $w_i V_i$ is the mass flow rate of the component i and L_v is the latent heat of vaporization (J/kg). The source term S_l is calculated thanks to the liquid and solid conservation equations leading to:

$$\left(\frac{1}{1 - \rho_v/\rho_l}\right)\frac{\partial w}{\partial t} = -\frac{\partial}{\partial x}\left(\delta_l \frac{\partial p_c}{\partial x}\right) + S_l \quad (4)$$

Equations (2), (3) and (4) describe the HM model. This set of equations is coupled, non-linear, and has to be solved numerically. For one dimensional problems, finite volumes and finite elements methods lead to the same discretized equations than the ones obtained with the finite difference method. Therefore the formalism of the latter is chosen. An implicit scheme is selected here based on Patankar (1980) and Patankar and Baliga (1978) work. The HM model was numerically solved with PYTHON for a non-uniform spatial discretization.

Boundary Conditions

External boundary conditions account for the convective heat and mass transfer with the outdoor air, radiative heat transfer and latent and sensible heat transfer due to vapor exchange. The external heat flux q_h is expressed as follows:

$$q_h = q_{h,conv} + q_{LWR} + q_{SWR} + q_{m,conv} \quad (5)$$

where $q_{h,conv}$, q_{LWR}, q_{SWR} are respectively the convective heat transfer, the long-wave radiation, the short-wave radiation and $q_{m,conv}$ gathers the latent and sensible heat transfer due to vapor exchange. The

convective heat exchange is given by Newton's law:

$$q_{h,conv} = h_{h,e}(T_e - T_{es}) \tag{6}$$

where $h_{h,e}$ is the convective heat transfer coefficient (CHTC, in W/(m^2.K)), subscripts e and es stand for exterior and exterior surface respectively. The CHTC is dominated by forced convection due to the wind. Hence, it depends on the measured local air velocity. Numerous empirical relationship linking the CHTC to the local air velocity exist; some can be found in Hagashima et al. (2005) and Loveday and Taki (1996). The one from Sharples (1984) is selected here:

$$\begin{gathered} h_{h,e} = 1.7V_{loc} + 5.1 \\ V_{loc} = 1.8V + 0.2\ (windward) \\ V_{loc} = 0.4V + 1.7\ (leeward) \end{gathered} \tag{7}$$

where V_{loc} is the local wind velocity (m/s) and V is reference wind speed (m/s). Moreover, this equation was also used by Janssen et al. (2007) after a comparison with various models.

The long-wave radiation is composed of the radiative exchanges with the ground and the sky:

$$q_{LWR} = \sigma\varepsilon F_{gro}(T_{gro}^4 - T_{es}^4) + \sigma\varepsilon F_{sky}(T_{sky}^4 - T_{es}^4) \tag{8}$$

where σ is the Stefan-Boltzmann constant (W/(m^2.K^4)), ε is the emissivity (-), F_{gro} and F_{sky} are the ground and sky view factors respectively (-). These coefficients are both equal to 0.5 each. The short-wave radiative transfer is given by equation (9):

$$q_{SWR} = \kappa(Dir + Dif + Ref) \tag{9}$$

κ is the absorptivity of the wall surface material (-), *Dir*, *Dif* and *Ref* are the direct radiation from the sun, the diffuse radiation by the atmosphere and the reflected radiation by the environment respectively (W/m^2). The latent and sensible heat transfer due to vapor exchange is:

$$q_{m,conv} = (c_{p,v}T_{es} + L_v)g_{conv} \tag{10}$$

where g_{conv} is the convective mass transfer flux calculated as follows:

$$g_{conv} = h_{m,e}(p_{v,e} - p_{v,es}) \tag{11}$$

where $h_{m,e}$ is the convective mass transfer coefficient kg/(m^2.s.Pa)). As the driving potential chosen here for the HM model at the wall scale is the capillary pressure, $p_{v,es}$ has to be expressed as a function of $p_{c,es}$ by using Gibbs' law:

$$g_{conv} = h_{m,e}\left[p_{v,e} - p_{sat}(T)exp\left(-\frac{p_{c,es}}{\rho_l R_v T_{es}}\right)\right] \tag{12}$$

where R_v is the ideal constant of water vapor (J/(kg.K)). For the surface moisture transfer coefficient, the Lewis' analogy is used (quoted by Janssen et al. (2007)):

$$h_{m,e} = 7.7 \times 10^{-9} h_{h,e} \tag{13}$$

Radiative heat transfer is not considered for the indoor boundary conditions and it is assumed that the CHTC is equal to 4 W/(m².K).

Indoor Conservation Equations

The indoor hygrothermal conditions depend on the interactions between the building and its surrounding environment. The temperature and water vapor pressure of a room are described by mass and energy balance equations. The model presented here assumes that the temperature and the water vapor pressure are uniform within the entire room volume.

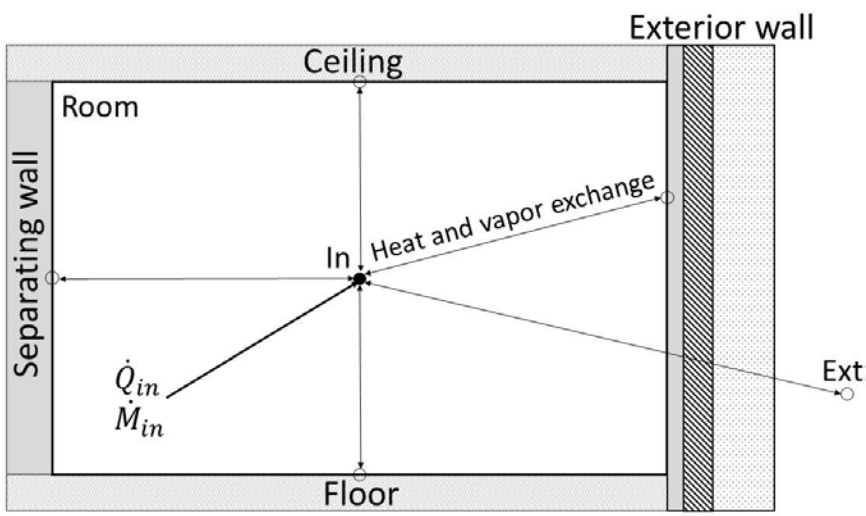

Figure 2: Scheme of the heat and mass transfer used to compute the balance for indoor air

The indoor air humidity is influenced by numerous parameters (Figure 2): humidity transfer from adjoining walls, water vapor exchange with the exterior due to the ventilation and water vapor production or losses due to the occupants' presence and activities. Consequently, the mass balance equation on the indoor air is:

$$\rho_a V \frac{\partial x_{in}}{\partial t} = \sum_j A_j h_{m,in}(p_{v,is,j} - p_{v,in}) + nV\rho_a(x_e - x_{in}) + \dot{M}_{in} \tag{14}$$

where ρ_a is the air density (kg/m³), V is the volume of the room (m³), subscript *in* refers to indoor, x_{in} is the mass ratio of the indoor air (-) defined as the mass of water vapor in one kilogram of dry air, A is the surface area of the wall j, n is the air change rate ACH (s⁻¹) $p_{v,is,j}$ is the surface water vapor pressure of the wall j and $\dot{M}_{in}$ is the indoor moisture sources/sinks. A similar expression can be found in Korjenic and Bednar (2012). To make equation (14) compatible with the boundary conditions, it needs to be expressed with the

water vapor pressure as potential. The mass ratio is linked to the water vapor pressure through the following equation:

$$x = \frac{R_a}{R_v} \cdot \frac{p_v}{p_{atm} - p_v} \tag{15}$$

where R_a is the ideal constant of the dry air (J/(kg.K)), p_{atm} is the atmospheric pressure (Pa). Combining equations (14) and (15) leads to:

$$\frac{R_a}{R_v} \cdot \frac{\rho_a V}{p_{atm} - p_{v,in}} \frac{\partial p_{v,in}}{\partial t} = A h_{m,in}(p_{v,is} - p_{v,in}) + \frac{R_a}{R_v} \cdot \rho_a n V . \left(\frac{p_{v,e}}{p_{atm} - p_{v,e}} - \frac{p_{v,in}}{p_{atm} - p_{v,in}} \right) + \dot{M}_{in} \tag{16}$$

Indoor heat balance is influenced by the convective transfer with adjoining walls, the air renewal and indoor heat sources (Tariku, 2008). Note that both sensible and latent contributions were included.

$$\begin{aligned} \rho_a C_{p,a} V \frac{\partial h}{\partial t} = & \sum_j A_j h_{h,in}(T_{is,j} - T_{in}) + n V \rho_a c_{p,a}(T_e - T_{in}) \\ & + (C_{p,v} T_{in} + L_v) \sum_j A_j h_{m,in}(p_{v,is,j} - p_{v,in}) \\ & + n V \rho_a [(C_{p,v} T_e + L_v) x_e - (C_{p,v} T_{in} + L_v) x_{in}] + \dot{Q}_{in} \end{aligned} \tag{17}$$

where h is the specific enthalpy (J/kg), $C_{p,a}$ is the heat capacity of the air (J/(kg.K)) and $T_{is,j}$ is the surface temperature of the wall j. The left term is expressed as a function of the temperature thanks to equation (18):

$$\frac{\partial h}{\partial t} = (C_{p,a} + x_{in} C_{p,v}) \frac{\partial T}{\partial t} \tag{18}$$

$\dot{Q}_{in}$ is a source/sink term regrouping all of the other heat losses or gains. It is decomposed as the sum of the sensible and latent loads:

$$\dot{Q}_{in} = \dot{Q}_{sen} + \dot{Q}_{lat} = \dot{Q}_{sen} + (c_{p,v} T_{in} + L_v) \dot{M}_{in} \tag{19}$$

$\dot{Q}_{sen}$ corresponds to the sensible heat due to the occupants' presence, the heating/cooling system and the use of lights.

Heating, Cooling and Ventilation Systems

As this work does not focus on a precise representation of a HVAC system, the heating and cooling systems are modelled to keep the indoor air temperature between 20 and 24 °C. The ventilation rate is taken equal to 0.5 air change per hour (ACH, in h^{-1}). According to Künzel et al. (2005b), it corresponds to the minimum

rate for German building standards, and according to Labat and Woloszyn (2015) it is also in agreement with the French code on building ventilation.

Modelling of Occupants' Presence

The occupants' presence is modelled in accordance with the model developed by Page et al. (2008). The presence (or absence) of an occupant is based on an inhomogeneous Markov chain using a parameter of mobility μ and a time-dependent profile of the probability of presence *P(t)* as input. This model generates a sequence of zeros (absence) or ones (presence) that characterize arrivals or departures from a zone for each occupant. These are obtained by calculating the probabilities of transition *T(t)*. For example, from absent to present (0 to 1):

$$\boldsymbol{T_{01}(t) = \frac{\mu - 1}{\mu + 1} P(t) + P(t+1)} \tag{20}$$

Or from present to present:

$$\boldsymbol{T_{11}(t) = \frac{P(t) - 1}{P(t)} \left[\frac{\mu - 1}{\mu + 1} P(t) + P(t+1)\right] + \frac{P(t+1)}{P(t)}} \tag{21}$$

The other two probabilities of transition are $T_{10} = 1 - T_{11}$ (from present to absent) and $T_{00} = 1 - T_{01}$ (from absent to absent). The parameter of mobility is defined as the ratio between the probability of change of the state of presence and that of no change. Here, this parameter is kept constant and equal to 0.11 based on Page's work to simplify the input (Page et al., 2008).

A metabolic heat gain is calculated using Fanger's PMV model (BS EN ISO 7730, 2005) and associated to each agent. This calculation is based on the metabolic rate, the clothing insulation and physical environmental parameters: air temperature, mean radiant temperature, air velocity and air relative humidity. For office buildings, the only activity considered is information technology (IT) where the clothing insulation coefficient is equal to 0.7 and the metabolic rate equal to 116 W/m^2. The air velocity is assumed constant and equal to 0.1 m/s. The mean radiant temperature is taken equal to the air temperature; the latter is calculated by solving equation (17). The indoor air water vapor pressure is calculated thanks to equation (16) and is then converted to the air relative humidity.

In this work, the occupants' presence model is integrated into a multi-agent stochastic simulation platform called No-MASS (Nottingham Multi-Agent Stochastic Simulation) (Chapman et al., 2017). This platform also integrates activity models for residential buildings from Jaboob (2015) and interactions between agents from Chapman (2017). These two points are not developed here as this paper focuses on occupants' presence in offices. No-MASS is then coupled with the HM model by using a Functional Mockup Interface (Figure 3).

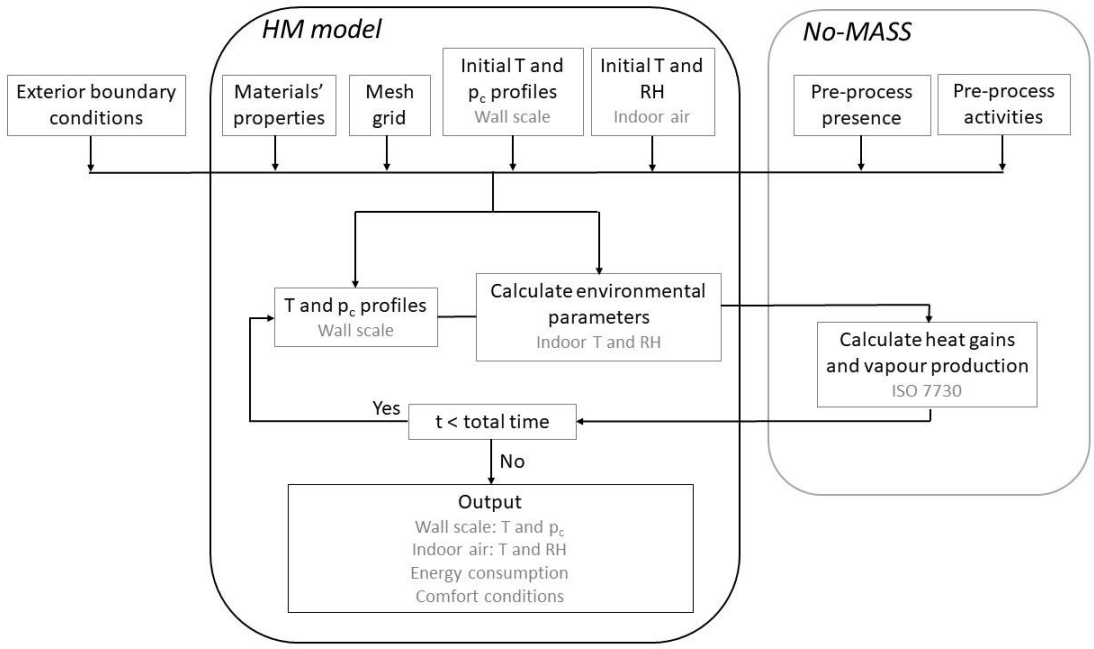

Figure 3: Scheme of the coupling between No-MASS and the HM model

First, the presence of agents in offices is pre-processed as it does not rely on environmental parameters. Next, the HM model calculates the environmental parameters, which are communicated to No-MASS. The latter is used to determine the metabolic heat gains and the water vapor production. The outputs from No-MASS are then parsed back to the HM model for the next time step until the end of the simulation.

As highlighted in Labat and Woloszyn (2015), various moisture production scenario can be found in the literature. It differs in terms of both the schedule (constant, cyclic, variable) and the intensity (from 20 to 500 g/h, depending on the room and its use). Here, as the occupants' presence is modelled in a stochastic way, cyclic or constant schedules are inappropriate. Contrary to what was done for sensible heat emitted by an occupant, there is no equivalent standard for vapor production, so a simplified modelling will be adopted here. In Simonson et al. (2001), a vapor production of 87 g/h was selected to simulate moisture production from two people sleeping. Note that it corresponds to 30 W of latent loads. This value also corresponds to a person seated at a theater according to ASHRAE (1997). Here, this value was selected as a first assumption as being seated in a theater might not be very different - in terms of moisture production - from the IT activity.

The electric lighting system model in No-MASS is based on the Lightswitch-2002 algorithm (Reinhart, 2004), which require calculated values of the indoor illuminance. However this was not included in our model yet. Consequently, it was assumed that the lights were turned on from 1 hour before sunset to 1 hour after sunrise if the room is occupied. A 10 W/m² heat gain is associated to the use of light, based on M. Steeman et al. (2009) work.

A time step sensitivity study led to choose a 5 minutes simulation time step for No-MASS (Chapman et al., 2017). For the HM model, an adaptive time step method is used. A list of the major parameters of the simulation is presented in Table 1.

MODELS VALIDATION

The presence model was calibrated and validated thanks to data provided by the monitoring of a twenty zones office building for five years (Page et al., 2008). For the coupled heat and mass transfer model at the wall scale, the validation relies on the standard BS EN 15026 (2007). This standard provides an analytical solution of coupled heat and mass transfer equations in a semi-infinite wall which is originally in equilibrium with its surrounding climate conditions at T=20°C and RH=50%. The specimen is then submitted to a temperature T=30°C and a relative humidity RH=95%. The test requires to plot the resulting water content and temperature profiles at different time step, namely 7, 30 and 365 days. The profiles are then compared to an analytical solution and should not deviate from more than 2.5% to pass. The material properties are specified in the standard. The semi-infinite wall was simulated by setting the wall thickness to 20 m. Figure 4 presents the water content and temperature distributions generated by the model.

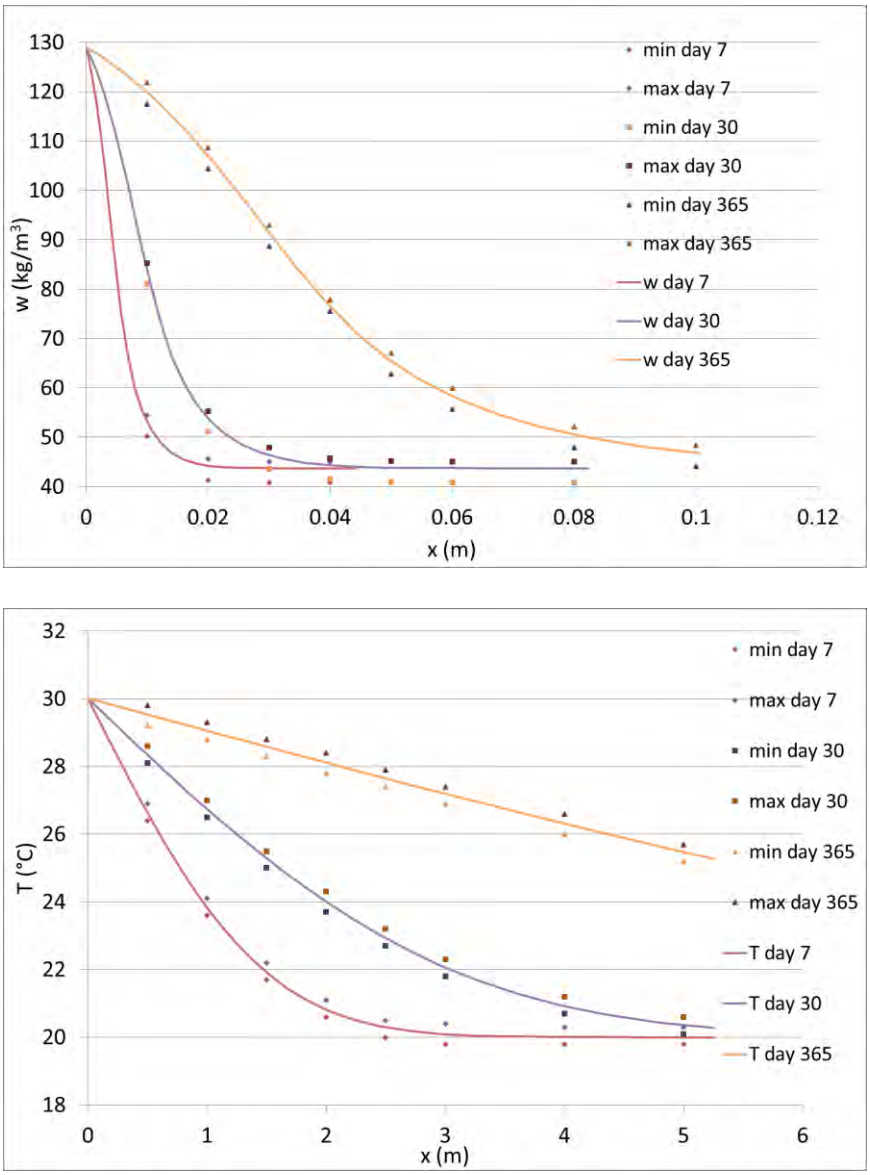

Figure 4: Water content (above) and temperature (below) distributions at 7, 30 and 365 days

Both profiles stay in the ±2.5% range from the analytical simulation (represented by the dots), meaning that the model passes this standard. Additionally, the maximum deviation from the analytical solution for the water content is 1.87% (corresponding to 0.80 kg/m^3) and 0.25% for the temperature (corresponding to 0.04°C) indicating a satisfactory accuracy.

SIMULATIONS

Case Study

A 5 m × 5 m × 2.5 m office room is simulated under the climatic conditions of Trappes (close to Paris, France), which is typical of the dominating climate of France (oceanic climate). It was assumed that this office was surrounded by similar offices except for one exterior wall facing the South direction. The separating walls are made of two 13 mm thick plasterboards. The floor and the ceiling are made of a load-bearing material (200 mm thick). It is assumed that all of the other offices surrounding the simulated room are at a constant temperature and relative humidity equal to 20°C and 40%RH respectively. In order to investigate the impact of the materials on the energy performance and the occupants' comfort, two distinct cases were studied with selecting different materials constituting the exterior wall. The first configuration consists of a conventional wall assembly made of 200 mm of concrete, 130 mm of polystyrene and 13 mm of plaster. This will be referred to as conventional wall (CW). The second configuration consists of a monolayer wall made of 390 mm of hemp concrete. This thickness was selected in order to have a thermal resistance close to the one from the first configuration (equal approximately to 3.40 (m^2.K)/W), but the hygroscopic properties differs significantly from the CW, as highlighted in the Annex. Therefore, this second case will be referred to as hygroscopic wall (HW).

The outdoor boundary conditions are given by the climate data file of the French thermal regulation RT 2012 (RT Bâtiment, 2012) which oversees new building construction in France. At the start of each of the two simulations, the office room is supposed to be initially at 20 °C and 40 %RH. A one year period is simulated (given in an hourly data file) starting from the 1st of January (under the assumption that it is a Monday for the occupants' schedule).

Occupancy Schedule

For the indoor sources, the presence of two agents in the simulated office was generated by No-MASS. The profile of occupants are typical of university workers. The average heat gain is calculated at each time step and then multiplied by the number of occupants. Note that the occupancy schedule is different for each occupant, meaning that there may be one or two person at the same time within the office. Figure 6 presents the metabolic heat gain generated by the occupants over a week. The moisture production schedule, not presented here, has a similar shape yet a constant 87 kg/h production rate per occupant was selected.

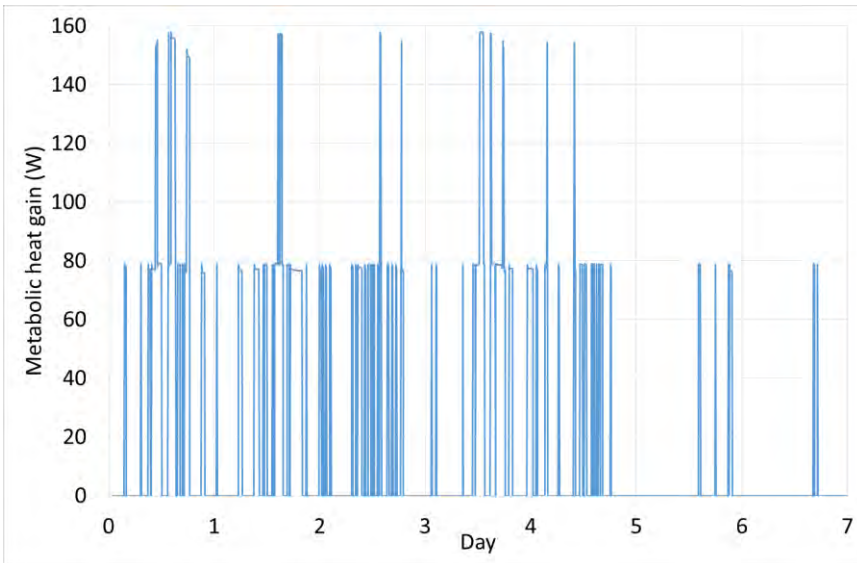

Figure 5: Computed metabolic heat gains over one week (January 1st - 7th)

Results

First, the impact of the materials on the energy consumption of the simulated room is studied through the energy demand for heating, as illustrated in Figure 6. For the sake of clarity, the values were averaged monthly.

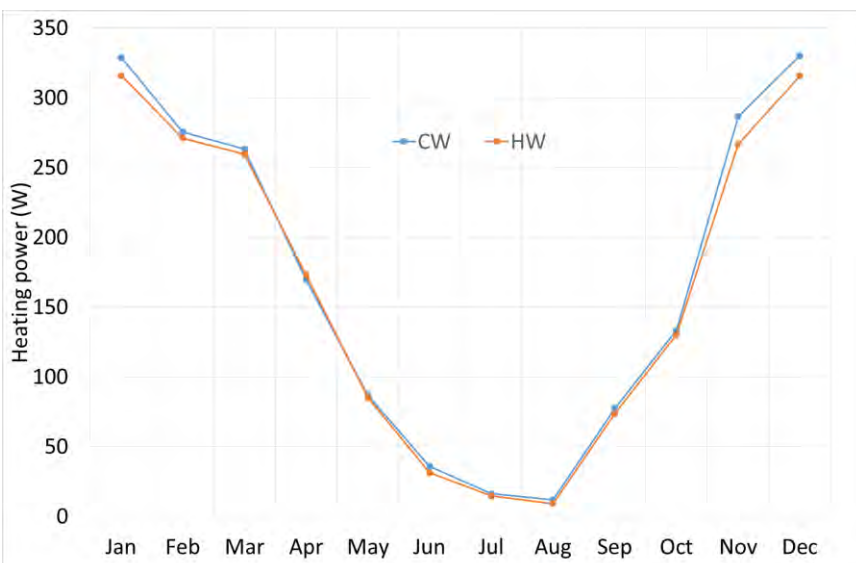

Figure 6: Monthly average heating power

The energy consumption was slightly lower (-3.6% in average) with the HW than with the CW despite both configurations having an almost equal thermal resistance (3.40 (m^2.K)/W). This can be explained by the difference in insulation: the CW has an interior insulation whereas the insulation is spread throughout the entire wall for the HW. Consequently, the indoor air temperature did not significantly change from one case study to the other and stayed in the range of 20-24°C as expected.

Next, indoor conditions were studied in detail. For example, the indoor relative humidity was plotted in Figure 7 for a typical winter week (January 1st – 7th) and summer week (July 1st – 7th).

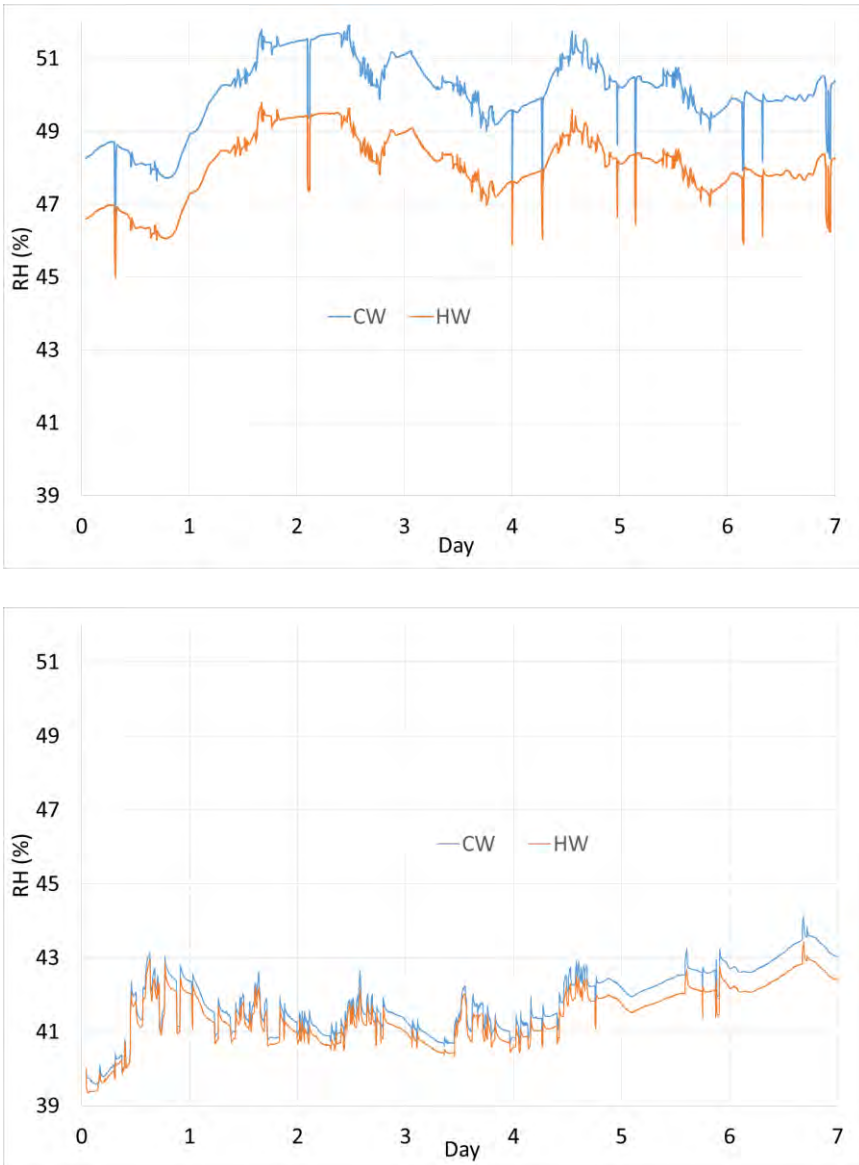

Figure 7: Indoor relative humidity. January 1st-7th (above) and July 1st-7th (below)

Both curves appear to be parallel. The HW leads, for each week, to a lower indoor relative humidity than the one calculated with the CW. The difference is very small during the winter week (maximum of 1%RH of difference). This is explained by the same initial conditions at the start of each simulation (1st of January). Still, this tendency is confirmed during the summer week where the difference can reach as much as 2.5%RH. This result might be due to the low water vapor resistance of the HW contrarily to the CW which is more impermeable to water vapor transfer. Indeed, the order of magnitude of the water vapor resistance of the HW is 10^9 m/s whereas it is 10^{11} m/s for the CW. For the summer week, the sudden drops in the plot correspond to a brief presence of occupants' in the office (less than 15 min) during hours when light are needed, and after a long period of absence (more than 4 hours). Heat is suddenly generated due to their presence and the use of light, leading to a decrease of RH. As the impact of the moisture production is low

in front of the heat generation, this drop was expected.

Figure 8 shows the indoor relative humidity distribution over a year for the CW and the HW in 2%RH intervals where the abscissa represents the mean value of each interval (meaning for example the abscissa 41 corresponds to the interval [40, 42]%RH).

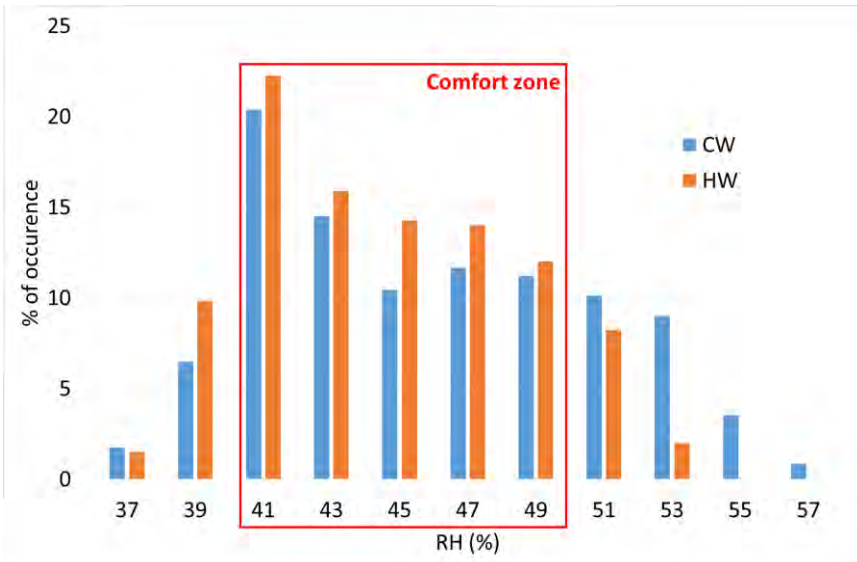

Figure 8: Indoor relative humidity distribution over a year

The indoor relative humidity distribution is consistent with the monthly results as the HW gives generally lower values of RH than the CW. In terms of comfort conditions, no relevant conclusion could be drawn with the calculation of the Predicting Mean Vote (PMV) and Predicted Percentage of Dissatisfaction (PPD) (BS EN ISO 7730, 2005). The HW gives a maximum PMV and PPD equal to 0.72 and 16.01% respectively against 0.74 and 16.44% for the CW. As their calculation is based on an energy balance equation, the impact of the indoor RH is limited. Consequently, it has been decided to use the comfort criterion from Wolkoff and Soren (2007). They define the comfort zone for targeted value of indoor relative humidity ranging from 40 to 50%. Based on this comfort criterion, the HW led to an increase of 10% in the prediction of the comfort range (78% against 68% for the CW). It is noted that the HW leads to a lower maximum RH value compared to the CW (54% against 58%). This result was also highlighted by Hameury (2005) when he compared a wall made of wood with permeable and impermeable indoor coating. However, it is not clear if the HW is able to moderate low RH as the indoor RH did not reach values below 36%. Finally, since the HW seems to moderate the indoor RH, potential energy savings can be done if a humidification/dehumidification is simulated.

CONCLUSION AND PERSPECTIVES

A coupled heat and moisture transfer model at the wall scale was developed and validated with a standard. This model is then coupled with a stochastic model of occupants' presence and activities called No-MASS via a Functional Mockup Interface. A two-people office was simulated on an entire year and was supposed to be located in Trappes, France. Two wall configurations were selected: a first simulation with a conventional exterior wall made of concrete, polystyrene and plaster; and a second simulation with an

exterior wall made of a hygroscopic material (hemp concrete).

The results highlighted that the HW gave a lower simulated indoor relative humidity compared to the CW due its higher resistance to water vapor. This led to an increase in the prediction of the comfort range. No significant differences were observed on the energy consumption of the office room. Indeed, the heating system simulated in this work was an ideal system and both walls' configuration were adapted to have a similar thermal resistance. Future work will investigate the modeling of a heating/cooling system based on the response of a real system. Moreover humidification and dehumidification systems will be modelled. Since the wall materials have a non-negligible impact on the indoor relative humidity, it is expected that the energy consumption of these systems will defer depending on the composition of the wall.

Future work on the occupants' impact will focus on simulating residential buildings where the inhabitants have more activities (cooking, showering, sleeping …). This part is already implemented in No-MASS and will be coupled with the HM model. Other activities (for both office and residential buildings) includes the use of blinds, windows and lights.

REFERENCES

ASHRAE, 1997. 1997 ASHRAE handbook - Fundamentals. Atlanta: American Society of Heating, Refrigerating and Air-Conditioning Engineers, Inc.

Barbosa, R.M., Mendes, N., 2008. Combined simulation of central HVAC systems with a whole-building simulation model. Energy Build. 40.

Bejan, A., 2004. Convection Heat Transfer, 3rd ed. Wiley & Sons, Inc.

BS EN 15026, 2007. Hygrothermal performance of building components and building elements - Assessment of moisture transfer by numerical simulation.

BS EN ISO 7730, 2005. Ergonomoics of the thermal environment - Analytical determination and interpretation of thermal comfort using calculation of the PMV and PPD indices and local thermal comfort criteria.

Chapman, J., 2017. Multi-agent stochastic simulation of occupants in buildings. The University of Nottingham.

Chapman, J., Siebers, P.-O., Robinson, D., 2017. On The Multi Agent Stochastic Simulation Of Occupants In Buildings. J. Build. Perform. Simul. (under review).

Delgado, Ramos, Barreira, Freitas, 2010. A critical review of hygrothermal models used in porous building materials. J. Porous Media 13, 231–234.

Diasty, E., Fazio, P., 1992. Modelling of indoor air humidity: the dynamic behaviour within an enclosure. Energy Build. 19, 61–73.

Evrard, A., 2008. Transient hygrothermal behaviour of lime-hemp materials. Université Catholique de

Louvain, Louvain, Belgique.

Gnip, I.Y., Veyalis, S.A., Kershulis, V.I., 2006. Isotherms of water vapor sorption by light inorganic and polymer heat-insulating materials. J. Eng. Phys. Thermophys. 69, 40–47.

Hagashima, A., Tanimoto, J., Ken-Ich, N., 2005. Intercomparison of experimental convective heat transfer coefficients and mass transfer coefficients of urban surfaces. Bound.-Layer Meteorol. 117, 551–576.

Haldi, F., Robinson, D., 2009. Interactions with window openings by office occupants. Build. Environ. 44, 2378–2395.

Hameury, S., 2005. Moisture buffering capacity of heavy timber structures directly exposed to an indoor climate: a numerical study. Build. Environ. 40, 1400–1412.

Jaboob, S., 2015. Stochastic modelling of occupants' activities and related behaviours. The University of Nottingham.

Janssen, H., 2014. Simulation efficiency and accuracy of different moisture transfer potentials. J. Build. Perform. Simul. 7, 379–389.

Janssen, H., Blocken, B., Carmeliet, J., 2007. Conservative modelling of the moisture and heat transfer in building components under atmospheric excitation. Int. J. Heat Mass Transf. 50, 1128–1140.

Janssens, A., 2001. Advanced numerical models for hygrothermal research: 2DHAV model description. Moisture Anal. Condens. Control Build. Envel. 40, 177–178.

Korjenic, A., Bednar, T., 2012. An analytical solution of a moisture transfer problem for coupled room and building component. Energy Build. 47, 254–259.

Künzel, H.M., 1995. Simultaneous Heat and Moisture Transport in Building Components - One- and two-dimensional calculation using simple parameters. Fraunhofer Institute of Building Physics, Stuggart, Allemagne.

Künzel, H.M., Kiesel, K., 1994. Calculation of heat and moisture transfer in exposed building components. J. Heat Mass Transf. 40, 159–167.

Künzel, H.W., Holm, A., Zirkelbach, D., Karagiozis, A.N., 2005a. Simulation of indoor temperature and humidity conditions including hygrothermal interactions with the building envelope. Energy Build. 78, 554–561.

Künzel, H.W., Holm, A., Zirkelbach, D., Karagiozis, A.N., 2005b. Simulation of indoor temperature and humidity conditions including hygrothermal interactions with the building envelope. Energy Build. 78, 554–561.

Labat, M., Magniont, C., Nicolaas, O., Aubert, J.-E., 2016. From the experimental characterization of the hygrothermal properties of straw-clay mixtures to the numerical assessment of their buffering potential. Build. Environ.

Labat, M., Woloszyn, M., 2015. Moisture balance assessment at room scale for four cases based on numerical simulations of heat-air-moisture transfers for a realistic occupancy scenario. J. Build. Perform. Simul.

Li, Q., Rao, J., Fazio, P., 2009. Development of HAM tool for building envelope analysis. Build. Environ. 44, 1065–1073. doi:10.1016/j.buildenv.2008.07.017

Lorente, S., 2017. The Constructal law as an approach to address energy efficiency in the urban fabric. Presented at the Constructal Law & Second Law Conference, Bucharest (Romania).

Loveday, D.L., Taki, A.H., 1996. Convective heat transfer coefficients at a plane surface on a full-scale building facade. Int. J. Heat Mass Transf. 39, 1729–1742.

Luikov, A.V., 1975. Systems of differential equations of heat and mass transfer in capillary-porous bodies. Int. J. Heat Mass Transf. 18, 1–14.

Page, J., Robinson, D., Morel, N., Scartezzini, J.-L., 2008. A generalised stochastic model for the simulation of occupant presence. Build. Environ. 40, 83–98.

Patankar, S.V., 1980. Numerical Heat Transfer and Fluid Flow. Hemisphere Publishing Corporation.

Patankar, S.V., Baliga, B.R., 1978. A New Finite-Difference Scheme for Parabolic Differential Equations. Numer. Heat Transf. Part B - Fundam. 1, 27–37. doi:10.1080/10407797809412159

Pedersen, C.R., 1990. Combined Heat and Moisture Transfer in Building Constructions. Technical University of Denmark, Denmark.

Perez-Lombard, L., Ortiz, J., Maestre, I., 2011. The map of energy flow in HVAC systems. Appl. Energy 88, 5020–5031.

Philip, J.R., De Vries, D.A., 1957. Moisture movement in porous materials under temperature gradients. Trans. Am. Geophys. Union 38, 222–232.

Qin, M., Belarbi, R., Aït-Mokhtar, A., Allard, F., 2009. Simulation of coupled heat and moisture transfer in air-conditioned buildings. Autom. Constr. 18, 624–631.

Qin, M., Walton, G., Belarbi, R., Allard, F., 2011. Simulation of whole building coupled hygrothermal-airflow transfer in different climates. Energy Convers. Manag. 52, 1470–1478.

Reinhart, C., 2004. Lightswitch-2002: a model for manual and automated control of electric lighting and blinds. Sol. Energy 77.

RT Bâtiment, 2012. RT neuf 2012: Données météorologiques [WWW Document]. URL http://www.rt-batiment.fr/batiments-neufs/reglementation-thermique-2012/donnees-meteorologiques.html (accessed 6.14.17).

Schellen, H.L., Van Schijndel, A.W.M., Briggen, P.M., 2008. The use of COMSOL for Building

Constructions Engineering regarding Heat and Moisture Transport, in: Excerpt from the Proceedings of the COMSOL Conference.

Sharples, S., 1984. Full-scale measurements of convective energy losses from exterior building surfaces. Build. Environ. 19, 31–39.

Simonson, C.J., Salonvaara, M.H., Ojanen, T., 2001. Moisture Content of Indoor Air and Structures in Buildings with Vapor-Permeable envelopes. Perform. Exter. Envel. Whole Build. VIII.

Steeman, H.-J., Van Belleghem, M., Janssens, A., De Paepe, M., 2009. Coupled simulation of heat and moisture transport in air and porous materials for the assessment of moisture related damage. Build. Environ. 44, 2176–2184.

Steeman, M., Janssens, A., De Paepe, M., 2009. Performance evaluation of indirect evaporative cooling using whole-building hygrothermal simulations. Appl. Therm. Eng. 29.

Tariku, F., 2008. Whole Building Heat and Moisture Analysis. Concordia University.

Tariku, F., Kumaran, K., Fazio, P., 2010. Transient model for coupled heat, air and moisture transfer through multilayered porous media. Int. J. Heat Mass Transf. 53, 3035–3044.

TenWolde, A., Walker, I., 2001. Interior Moisture Design Loads for Residences, in: Proceedings of Thermal Performance of Exterior Envelopes of Buildings VIII, ASHRAE. Atlanta, GA.

Walton, G.N., 1989. AIRNET - A computer program for building airflow network modelling. National Institute of Standards and Technology.

Wolkoff, P., Soren, K.K., 2007. The dichotomy of relative humidity on indoor air quality. Environ. Int. 33, 850–857.

Woloszyn, M., Rode, C., 2008. Tools for performance simulation of heat, air and moisture conditions of whole buildings. Build. Simul. 1, 5–24.

Woloszyn, M., Rode, C., 2007. IEA Annex41, MOIST-ENG, Subtask 1 - Modelling Principles and Common Exercices. Final Rep.

ANNEX

Table 1: Listing of the major parameters of the simulations

Major assumptions	No air transfer No rain simulated Opaque wall, no window simulated
Time step	Adaptive time step method for the HM model

	5 min time step for No-MASS
Exterior boundary conditions	Convective heat and mass transfer Long-wave and short-wave radiation Latent and sensible heat transfer due to vapor exchange
Indoor heat sources	Heating system Occupants' presence and activity (around 80 W per occupant in offices) Use of light (10 W/m^2)
Indoor moisture sources	Occupants' presence and activities (87 g/h per occupant in offices)

Table 2: Materials properties extracted from the literature

Material	ρ (kg.m^{-3})	k (W.m^{-1}.K^{-1})	C_p (J.kg^{-1}.K^{-1})	δ_v*10^{-11} (s) dry cup	δ_v*10^{-11}	δ_v*10^{-11} (s) wet cup
Concrete (1)	2450	2.00	1000	0.15		0.24
Polystyrene (1)	50	0.04	1450		0.32(3)	
Plaster (1)	875	0.25	1000	1.90		4.75
Hemp concrete (2)	440	0.115	1560		5(3)	

Table 3: Sorption properties

Concrete (1)	**RH (%)** **w (kg/m^3)**	20 86	40 110	60 159	80 270	95 441		
Polystyrene (1)	**RH (%)** **w (kg/m^3)**	20 4	40 8	60 13	80 17	90 20	97 27	
Hemp concrete (2)	**RH (%)** **w (kg/m^3)**	0 0	32 14	50 20	65 28	80 33	93 42	96 62

Plaster (Gnip et al., 2006): $w = \rho \times 0.077(1 + |-215.23 \ln(RH)|^{1.628})^{-1+\frac{1}{1.628}}$

Table 4: Liquid water permeability

Concrete	**δ_l (s)** (4)	10^{-17}		
Polystyrene	**w (kg/m^3)** **δ_l (s)** (4)	13 10^{-17}	20 10^{-15}	27 10^{-14}

Plaster	**w (kg/m^3)** **δ_l (s)** [4]	0.04 10^{-17}	0.12 10^{-15}	0.20 10^{-14}
Hemp concrete [2]	**w (kg/m^3)** **δ_l (s)**	28 10^{-17}	42 10^{-15}	62 10^{-14}

[1] from (Labat et al., 2016)
[2] from (Evrard, 2008)
[3] single value given
[4] assumption – no value available